ON THE SHAPE AND STABILITY OF A CONDUCTING FLUID DROP ROTATING IN AN ELECTRIC FIELD

by

RUSSEL R. RANDALL

B.A., Kansas State Teachers College, 1970

A MASTER'S THESIS

submitted in partial fulfillment of the

requirements for the degree

MASTER OF SCIENCE

Department of Physics

KANSAS STATE UNIVERSITY
Manhattan, Kansas

1973

Approved by:

C. E. Rosenkilde
Major Professor

TABLE OF CONTENTS

I. INTRODUCTION

Many recent studies have involved the behavior of fluids in the presence of various internal and external fields of force. The earliest of these investigations involved the equilibrium and stability of self-gravitating fluid structures under the effects of rotation. Chandrasekhar[1] has extended these investigations to rotating fluid drops under the influence of a constant surface tension. There also have been similar studies of non-rotating dielectric fluid drops in uniform electric fields by Taylor[2] and Rosenkilde.[3] In this paper we shall draw from two of the previous investigations and consider the equilibrium and stability of an isolated conducting fluid drop with constant surface tension which is rotating in an uniform external electric field. This paper clarifies and extends the investigation of equilibrium shapes given by Habip, Siekmann, and Chang.[4]

The method of the tensor virial, which has been developed by Chandrasekhar,[5] provides the basis for the ensuing investigation. Spherical, spheroidal, and ellipsoidal shapes are shown to satisfy the first twelve moments of the hydrodynamical equation of motion. A linear, one parameter (the elongation) family of equilibrium curves for spheroidal shapes is obtained on a configuration plane. In this configuration plane, the ordinate represents the square of the angular momentum and the abscissa represents the electrostatic energy of possible spheroidal equilibrium configurations. The stability of these equilibrium shapes with respect to second-harmonic deformations is investigated by using a normal-mode analysis based upon linearized perturbations of the

time-dependent moment equations. Stable spheroidal configurations are shown to be restricted to a closed region in this configuration plane. The anlysis of the normal mode closely resembles the one given by Lebovitz[6] for the classical Maclaurin spheroids and Jacobi ellipsoids.

The general moment equations are derived in Section II by making an appropriate extension of the corresponding derivation given by Rosenkilde[3] for a nonrotating dielectric fluid drop. In Section III, these moment equations are reduced to the form that describes a state of static equilibrium, as viewed from the rotating frame of reference in which the surface is at rest. The resulting equations are evaluated and analyzed for ellipsoidal shapes by using expressions that are summarized in Appendix B. Expressions given there for a conductor have been obtained from those for a dielectric in the limit that the dielectric permeability approaches infinity. Section IV contains the general form taken by the moment equations that describe small oscillations about an equilibrium configuration. The resulting characteristic value problem is analyzed in Section V. Conditions for the onset of instability are obtained by examining the nature of the characteristic frequencies of oscillation. Numerical results and comparisons are presented in Section VI. Appendix A contains a complete summary and discussion of the various dimensional units and nondimensional parameters that are used throughout the text.

II. MOMENT EQUATIONS

Consider an uniformly rotating dielectric fluid drop situated in an uniform external electric field, with the axis of rotation along the direction of the electric field at infinity. After transforming to a coordinate frame rotating about the x_3 axis with a constant angular speed Ω, the hydrodynamical equation* describing the motion of an arbitrary fluid element is

$$\rho \frac{d}{dt} u_i - 2\rho\Omega\epsilon_{i\ell 3} u_\ell = \frac{\partial \sigma_{ik}}{\partial x_k} - \frac{\partial p}{\partial x_i} + \rho\Omega^2\left[x_i - \delta_{i3} x_3\right], \quad (2.1)$$

where ρ is the mass density of the fluid, $\underline{u}$ is the mean velocity of a fluid element, p is the hydrostatic pressure, and σ_{ik} is an appropriate stress tensor.

A set of moment equations can be constructed by multiplying the above equation by x_j, and then formally integrating over the volume containing the fluid drop. The result is

$$\begin{aligned} \int_V \rho x_j \frac{du_i}{dt}\, d\tau - 2\Omega\epsilon_{i\ell 3}\int_V \rho u_\ell x_j\, d\tau \\ = \int_V x_j \frac{\partial \sigma_{ik}}{\partial x_k}\, d\tau - \int_V x_j \frac{\partial p}{\partial x_i}\, d\tau \\ + \Omega^2 \int \left[x_i x_j - \delta_{i3} x_j x_3\right]\rho\, d\tau . \end{aligned} \quad (2.2)$$

*The summation convention on repeated indices applies here as well as in the rest of the paper, unless otherwise stated.

These integral relations depend upon the second moments of the mass distribution

$$I_{ij} \equiv \int_V x_i \, x_j \, \rho \, d\tau \tag{2.3}$$

and their time derivatives. By using the equation of continuity, one obtains

$$\int_V \rho x_j \frac{du_i}{dt} d\tau = \frac{d}{dt}\int_V \rho x_j \, u_i \, d\tau - 2\,\mathcal{T}_{ij} \quad , \tag{2.4}$$

where

$$\mathcal{T}_{ij} \equiv \frac{1}{2}\int_V \rho \, u_i u_j \, d\tau \tag{2.5}$$

is the kinetic-energy tensor. The trace of $\mathcal{T}_{ij}$ is the macroscopic kinetic energy of the fluid. By symmetrizing the relation (2.4) one may obtain an expression which involves the second time derivative of I_{ij}.

The remaining terms in Eq. (2.2) may be rewritten in more recognizable physical forms. By using the divergence theorem,

$$\int_V x_j\left(\frac{\partial \sigma_{ik}}{\partial x_k} - \frac{\partial p}{\partial x_i}\right) d\tau = \int_S x_j\left[\sigma_{ik}^{(-)} n_k - p^{(-)} n_i\right] dS$$

$$+ \delta_{ij}\,\Pi - \int_V \sigma_{ij}\, d\tau \,, \tag{2.6}$$

where the superscript (-) is associated with quantities evaluated just inside the bounding surface S whose outward normal is $\underline{n}$. The quantity

$$\Pi = \int_V p \, d\tau \tag{2.7}$$

involves the remaining kinetic energy associated with the microscopic internal motion of the fluid particles within the drop. The hydrostatic pressure $p^{(+)}$ and the stress tensor $\sigma_{ik}^{(+)}$ just outside the bounding surface are related to the corresponding quantities just inside this surface by the condition

$$\sigma_{ik}^{(-)} n_k - p^{(-)} n_i = \sigma_{ik}^{(+)} n_k - p^{(+)} n_i - T\left(\nabla \cdot \underline{n}\right) n_i \quad , \tag{2.8}$$

where T is the constant surface tension. By using this boundary condition with $p^{(+)}$ set to zero (i.e., the drop is isolated), the surface integral in Eq. (2.6) becomes

$$\int_S x_j \left[\sigma_{ik}^{(-)} n_k - p^{(-)} n_i\right] dS = \mathcal{F}_{ij} - T \int_S x_j \left(\nabla \cdot \underline{n}\right) n_i \, dS \tag{2.9}$$

where

$$\mathcal{F}_{ij} \equiv \int_S x_j \, \sigma_{ik}^{(+)} n_k \, dS \tag{2.10}$$

is the moment of the external normal stress on S . The quantity

$$\sigma_{ik}^{(+)} = -\frac{1}{8\pi}\left[\underline{E}^{(+)}\right]^2 \delta_{ik} + \frac{1}{4\pi} E_i^{(+)} E_k^{(+)} \tag{2.11}$$

is the usual Maxwell stress tensor associated with the exterior electric field $\underline{E}^{(+)}$ on S. The contribution involving surface tension may be rewritten in the form

$$T \int_S \kappa_j (\nabla \cdot \underline{n}) n_i \, dS = 2 \mathcal{S}_{ij} \quad , \tag{2.12}$$

where

$$\mathcal{S}_{ij} \equiv \frac{1}{2} T \int \left[\delta_{ij} - n_i n_j \right] dS \tag{2.13}$$

is the surface-energy tensor (cf. Rosenkilde).[3]

The dielectric is assumed to be isotropic and homogenous so that the dielectric permeability ϵ is a scaler and is at most a function of the density ρ of the fluid. In the interior of the drop the appropriate stress tensor (cf. Landau & Lifshitz,[7] Eq. (15.9)) is

$$\sigma_{ij} = -\frac{1}{8\pi} \epsilon \left| \underline{E} \right|^2 \delta_{ij} + \frac{1}{4\pi} \epsilon E_i E_j \quad , \tag{2.14}$$

where $\underline{E}$ is the interior electric field. The additional diagonal contribution due to electrostriction included by Rosenkilde[3] has been suppressed here in anticipation of specialization to the conducting limit. For the systems of interest, $\Omega \cdot$ (typical radius)/(speed of light) $\ll 1$ so that the induced magnetic field arising from the rotation of the fluid drop may be ignored in the first approximation.

By using the expression (2.14), the remaining volume integral in Eq. (2.6) becomes

$$-\int_V \sigma_{ij}\, d\tau = \mathcal{E}\,\delta_{ij} - 2\,\mathcal{E}_{ij} \quad , \tag{2.15}$$

where

$$\mathcal{E}_{ij} \equiv \frac{1}{8\pi}\int \epsilon\, E_i\, E_j\, d\tau \quad , \tag{2.16}$$

is the electrostatic-energy tensor whose trace is $\mathcal{E}$.

Finally, the resulting moment equations are

$$\begin{aligned} &\frac{d}{dt}\int_V \rho\, x_j\, u_i\, d\tau - 2\Omega\epsilon_{i3}\int_V \rho\, u_i\, x_j\, d\tau \\ &= 2\,\mathcal{T}_{ij} + \Omega^2\left[I_{ij} - \delta_{i3}\, I_{3j}\right] + \Pi\,\delta_{ij} - 2\,\mathcal{S}_{ij} + \mathcal{W}_{ij} \quad , \end{aligned} \tag{2.17}$$

where

$$\mathcal{W}_{ij} \equiv \mathcal{T}_{ij} + \mathcal{E}\,\delta_{ij} - 2\,\mathcal{E}_{ij} \quad , \tag{2.18}$$

includes the various electrostatic contributions. They represent a set of nine time-dependent equations for the second moments of the mass distribution. By adding the three equations for which i=j, and ignoring rotation (as a special case), one obtains

$$\frac{d}{dt}\int_V \rho\, x_i\, u_i\, d\tau = 2\,\mathcal{T} - 2\,\mathcal{S} + \mathcal{W} + 3\,\Pi \tag{2.19}$$

where $\mathcal{T}$, $\mathcal{S}$, and $\mathcal{W}$ are, respectively, the kinetic, surface, and electrostatic contributions of the fluid. This relation, originally due to Lagrange and Jacobi, is a more general form of the virial theorem

later derived by Clausius (cf. Chandrasekhar,[8] chapt. 13). In view of this similarity, the moment equations (2.17) are also known collectively as the tensor virial-theorem.

The formal volume integral of the equation of motion (obtained without first multiplying by x_j) yields the conservation law for linear momentum. The nine moment equations just obtained imply the conservation of angular momentum and a generalization of the virial theorem. Successive sets of moment equations may be generated by repeating this process with $x_i x_j x_k \cdots$. This infinite sequence of sets of equations replaces the original equation of motion. In this paper the dynamics of the fluid drop will be approximated by satisfying only the lowest nontrivial set describing the second moments.

III. EQUILIBRIUM CONFIGURATIONS

Assume that the equilibrium configurations of the dielectric fluid drop are initially rotating uniformly with constant angular speed Ω, and that these configurations are initially at rest within the chosen frame of reference. The moment equations (2.17) must be satisfied when no relative motions are present and hydrostatic equilibrium prevails. Under these conditions, all velocities and time derivatives vanish. These equations reduce to

$$0 = \Omega^2\left[I_{ij} - \delta_{i3} I_{3j}\right] - 2\mathcal{S}_{ij} + \mathcal{F}_{ij} - 2\mathcal{E}_{ij} + \left(\mathcal{E} + \Pi\right)\delta_{ij} , \tag{3.1}$$

where $\mathcal{W}_{ij}$ has been replaced by its equivalent. Equations (3.1) represent a total of nine equations.

The application of the moment method requires, initially, the selection of a trial shape that is compatible with the moment equation of lowest order. It is known that the equilibrium configurations of a slowly rotating fluid drop acting under the influence of surface tension alone are nearly spheroidal.[1] It is also known that the equilibrium configurations of a stationary dielectric fluid drop in a small uniform electric field are nearly spheroidal.[2] In view of these results it is natural to try, initially, to represent the equilibrium configurations in the present case by spheroidal shapes. Therefore, the equilibrium configurations will be explicitly assumed to have ellipsoidal surfaces

of the form defined by Eq. (A.1). For the sake of convenience, these surfaces have initially been chosen to be tri-axial having nondimensional semiaxes a_1, a_2, and a_3. (All dimensional units are defined in Appendix A.)

The surface energy tensor $\mathcal{S}_{ij}$ is diagonal for an ellipsoid.[9] If the ellipsoidal body is assumed to rotate about one of the principal axes (hereafter identified as the third axis), then the off-diagonal elements of the moment of inertia tensor vanish. Under these conditions the six moment equations for which $i \neq j$ reduce to

$$\mathcal{T}_{ij} = 2\,\mathcal{E}_{ij} \qquad (i \neq j). \tag{3.2}$$

In order to explore the consequences of this requirement, it is useful to obtain a more explicit expression for the tensor evaluated for ellipsoical surfaces.

From the electrostatic boundary conditions

$$\underline{n}\cdot\left[\underline{\underline{E}}^{(+)} - \epsilon\,\underline{\underline{E}}^{(-)}\right] = 0 \qquad \text{and} \qquad \underline{n}\times\left[\underline{\underline{E}}^{(+)} - \underline{\underline{E}}^{(-)}\right] = 0\,, \tag{3.3}$$

it follows that

$$\underline{\underline{E}}^{(+)} = \underline{\underline{E}}^{(-)} + (\epsilon - 1)\left(\underline{n}\cdot\underline{\underline{E}}^{(-)}\right)\underline{n}\,. \tag{3.4}$$

This relation may be used to express the quantity

$$\begin{aligned} 8\pi\,\sigma_{ik}^{(+)}\,n_k = {} & \left[(\epsilon-1)^2\left(\underline{n}\cdot\underline{\underline{E}}^{(-)}\right)^2 - \left|\underline{\underline{E}}^{(-)}\right|^2\right] n_i \\ & + 2\epsilon\left[\underline{n}\cdot\underline{\underline{E}}^{(-)}\right] E_i^{(-)} \end{aligned} \tag{3.5}$$

in terms of $\underline{E}^{(-)}$ instead of $\underline{E}^{(+)}$ (cf. Eq. (2.11)). The substitution of Eq. (3.5) into the definition (2.10) leads to the general expression

$$\mathcal{F}_{ij} = \frac{1}{8\pi}\int_S \varkappa_j \left[2\epsilon(\underline{n}\cdot\underline{E})E_i - \left[|\underline{E}|^2 - (\epsilon-1)^2(\underline{n}\cdot\underline{E})^2\right] n_i \right] dS \ , \tag{3.6}$$

where the superscript (-) on $\underline{E}$ has been suppressed for the sake of simplicity.

When an ellipsoidal dielectric is placed in an uniform electric field $\underline{F}$, the resulting $\underline{E}$ within the dielectric is also uniform regardless of the orientation of the ellipsoid.[7] Thus the assumption of an ellipsoidal surface simplifies the evaluation of the electrostatic tensors, $\mathcal{F}_{ij}$ and $\mathcal{E}_{ij}$. Equations (3.2) become

$$0 = -2\mathcal{E}_{ij} + \mathcal{F}_{ij} = -\frac{\epsilon}{4\pi} E_i E_j \int_V d\tau$$

$$+ \frac{\epsilon}{4\pi} E_i E_l \int_S n_l \varkappa_j \, dS - \frac{1}{8\pi} E^2 \int_S \varkappa_j n_i \, dS \tag{3.7}$$

$$+ \frac{(\epsilon-1)^2}{8\pi} E_l E_m \int_S \varkappa_j n_l n_m n_i \, dS \ .$$

These equations may be further simplified by using the relation

$$\int_S \varkappa_p n_q \, dS = \delta_{pq} \int_V d\tau \ , \tag{3.8}$$

which follows from the divergence theorem. One then obtains

$$0 = -2\mathcal{E}_{ij} + \mathcal{F}_{ij} = \frac{(\epsilon-1)^2}{4\pi} E_i E_j \int_S n_i^2 (n_j \varkappa_j) \, dS \ , \tag{3.9}$$

(no sum)

since the last integral in Eq. (3.7) vanishes unless l=j and m=i or l=i and m=j due to the tri-planer symmetry of the ellipsoidal surface.

The integral in expression (3.9) is not zero. Therefore the requirement (3.9) cannot be satisfied unless two of the three components of $\underline{E}$ are zero. This is possible only if $\underline{E}$ is parallel to the axis of rotation. With this, together with the above assumptions, the six "off-diagonal" equations (3.1) are satisfied.

The remaining three diagonal equations (for which i=j) are

$$\begin{aligned} \Omega^2 I_{11} &= \Pi + 2\mathcal{S}_{11} - {}^3\mathcal{W}_{11} , \\ \Omega^2 I_{22} &= \Pi + 2\mathcal{S}_{22} - {}^3\mathcal{W}_{22} , \\ 0 &= \Pi + 2\mathcal{S}_{33} - {}^3\mathcal{W}_{33} . \end{aligned} \tag{3.10}$$

These equations must be satisfied simultaneously in order to relate the field strength and the amount of rotation to the shape. The last equation of the set (3.10) is used to eliminate the quantity Π from the remaining two equations. One obtains

$$\begin{aligned} \Omega^2 I_{11} &= \left[2\mathcal{S}_{11} - 2\mathcal{S}_{33}\right] - \left[{}^3\mathcal{W}_{11} - {}^3\mathcal{W}_{33}\right] , \\ \Omega^2 I_{22} &= \left[2\mathcal{S}_{22} - 2\mathcal{S}_{33}\right] - \left[{}^3\mathcal{W}_{22} - {}^3\mathcal{W}_{33}\right] . \end{aligned} \tag{3.11}$$

In order to explore the consequences of these two equations it is necessary to evaluate the tensors I_{ii}, ${}^3\mathcal{W}_{ii}$, and $\mathcal{S}_{ii}$ for ellipsoidal configurations. The results of this evaluation are summarized in

Appendix B. The required expressions involve multi-indexed symbols, such as A_{13} and A_2, which represent particular members of certain classes of elliptic integrals (which are also defined in Appendix B). By using Eqs. (B.1), (B.5), (B.6), (B.9), and (B.10), the equilibrium relations (3.11) become

$$\frac{1}{2} I^{\circ} \Omega^2 a_1^2 = \frac{1}{2} E_s^{\circ} \left[a_3 - a_1 \right] - E_c A_3^{-1} \left[a_1^2 A_{13} - 3 a_3^2 A_{33} \right]$$

$$\frac{1}{2} I^{\circ} \Omega^2 a_2^2 = \frac{1}{2} E_s^{\circ} \left[a_3 - a_2 \right] - E_c A_3^{-1} \left[a_2^2 A_{23} - 3 a_3^2 A_{33} \right] , \tag{3.12}$$

where the units of the moment of inertia I°, the surface energy E_s°, and the electrostatic energy E_c are defined in Appendix A. This pair of equations associates a definite angular momentum and electrostatic energy with a given ellipsoidal shape characterized by the pair of ratios, a_1/a_3 and a_2/a_3. Further discussion of these shapes will be deferred to Section VA.

Since the equilibrium configurations are expected to be nearly spheroidal in the limit of small fields or slow rotation, this case will be examined first. The spheroidal configurations are expected to rotate about their axis of symmetry, a_3. By replacing a_2 by a_1 wherever it occurs in Eqs. (3.12), one finds that these two equations become identical. They reduce to the single expression

$$y = \frac{1}{2} a_1^2 \left[a_3 - a_1 \right] - a_1^2 A_3^{-1} \left[a_1^2 A_{13} - 3 a_3^2 A_{33} \right] \varkappa , \tag{3.13}$$

where the electrical parameter χ and the rotational parameter y are explicitly defined in Appendix A.

The electrical parameter χ represents the electrostatic energy of the configuration expressed in units of the surface energy, E_s°, of a reference sphere having the same mass and volume as the spheroidal configuration. The rotational parameter y represents the square of the angular momentum of the equilibrium configuration expressed in units associated with the same reference sphere.

Spheroidal shapes are completely specified by a single parameter, the elongation $k = a_3/a_1$, where a_3 is the semimajor axis of symmetry. The coefficients in Eq. (3.13) are functions of the elongation. Hence, this expression implies a linear relationship between the physical parameters, χ and y, for a given spheroidal equilibrium shape.

Representative members of this one-parameter family of straight lines are shown in Fig. 1. The line representing the spherical shape (labeled k =1.0) extends diagonally from the origin. Each point on this line associates a particular amount of angular momentum and electrostatic energy with the same spherical equilibrium configuration with a given mass and volume. All along this "spherical" line the rotational forces that tend to flatten the configuration are opposed by the induced electrical stresses in such a way that the resulting equilibrium configuration remains spherical.

The configurations, which comprise the ordinate, form the sequence of oblate spheroidal shapes that approximate the exact figures of equilibrium obtained by Rayleigh[10] and Chandrasekhar.[1] (The quality of this approximation will be examined in Section VI.) In the absence of any applied electric field (χ =0), the configurations possessing more angular momentum require additional flattening in the polar regions in order to generate sufficient curvature (and hence interfacial tension) along the equation to counter balance the centrifugal spreading. All of the configurations that lie in the region to the right of the ordinate and above the "spherical" line are oblate ($k<1$). For a given angular momentum, y, in this region, an increase in electrostatic energy ($\chi > 0$), concentrates the induced polarization charge density and electrical stress in the polar regions while diminishing these near the equation so as to combine with the interfacial tension to reduce the oblateness caused by rotation.

The configurations which comprise the abscissa form the sequence of prolate spheroidal shapes that have been investigated by Taylor[2] and Rosenkilde.[3] As the electrostatic energy is increased in the absence of

FIG. 1. Linear equilibrium relations between the electrical parameter, α , and the rotational parameter, y , for selected values of the elongation, k , between 0.6 and 10.0.

THIS BOOK CONTAINS NUMEROUS PAGES WITH DIAGRAMS THAT ARE CROOKED COMPARED TO THE REST OF THE INFORMATION ON THE PAGE.

THIS IS AS RECEIVED FROM CUSTOMER.

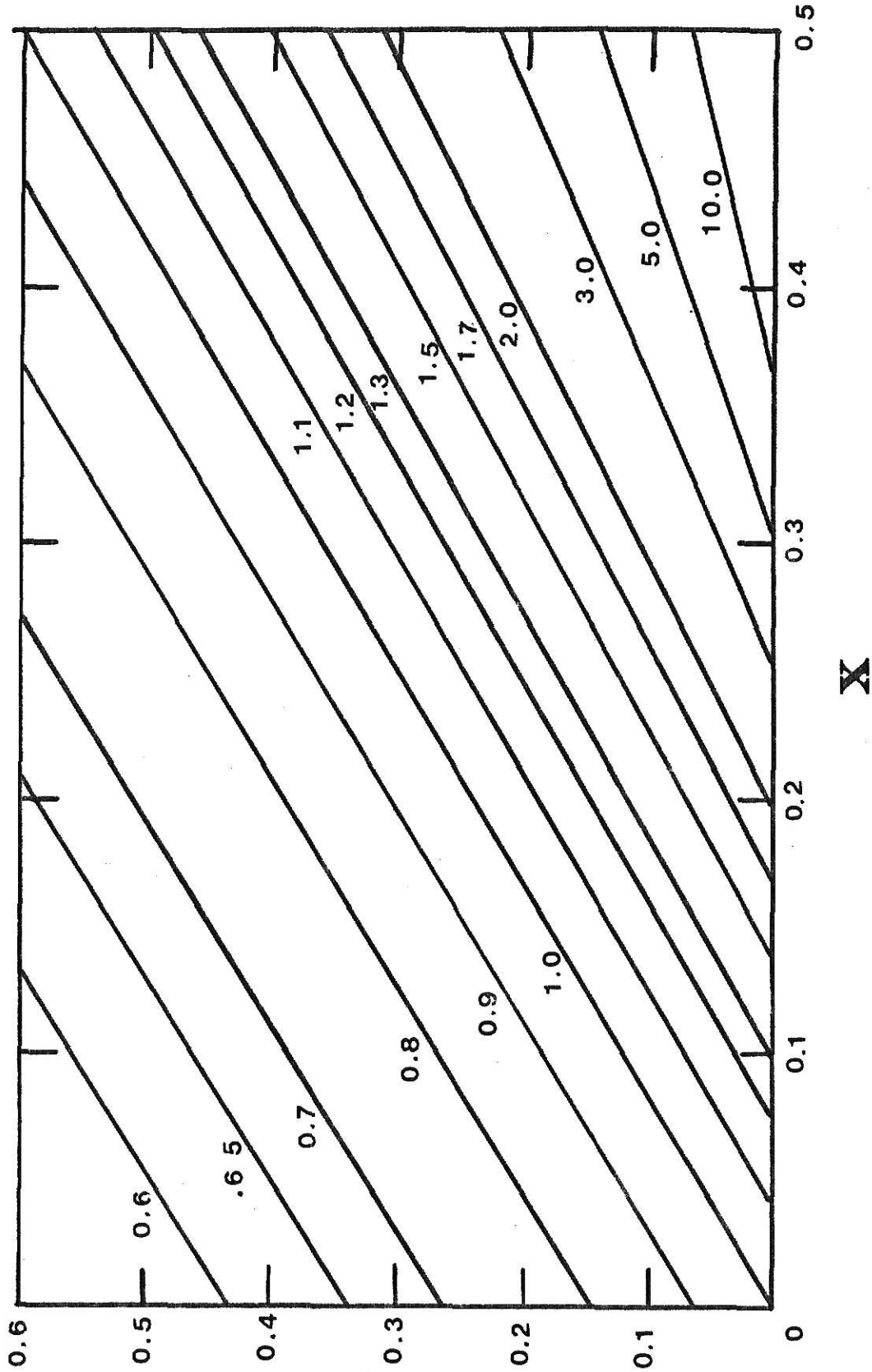
0.6
0.5
0.4
0.3
0.2
0.1
0
y
0.1
0.2
0.3
0.4
0.5
x
0.6
.6 5
0.7
0.8
0.9
1.0
1.1
1.2
1.3
1.5
1.7
2.0
3.0
5.0
10.0

any rotation (y =0), these configurations must yield to some elongation in the polar regions in order to generate sufficient curvature (and hence interfacial tension) there to counter balance the induced electrical stress. All of the configurations that lie in the region above the abscissa and to the right of the "spherical" line are prolate ($k > 1$). In this region the centrifugal force combines with the surface tension to reduce the elongation caused by electrical stress.

Although equilibrium configurations obtain throughout the entire first quadrant of this x-y configurative plane (for this spheroidal approximation), it is known that these configurations cannot all be stable. In particular, those configurations along the ordinate and the abscissa that are unstable with respect to second-harmonic deformations have been identified by Chandrasekhar[1] and Rosenkilde,[3] respectively, using normal-mode analyses based upon small variations in moment equations corresponding to appropriate limiting cases of Eqs. (2.17). On this account one may expect some bounds on the possible stable configurations in this plane.

IV. VIRIAL EQUATIONS OF SMALL OSCILLATIONS ABOUT EQUILIBRIUM

The moment equations (2.17) will be used to investigate the stability of the spheroidal equilibrium configurations with respect to second-harmonic deformations. Conditions for the onset of instability will follow from an examination of the nature of the characteristic frequencies of oscillation associated with these deformations. The normal mode analysis to be given here for a conducting spheroid that is rotating in the presence of an electric field closely resembles earlier analyses of rotating fluid configurations given by Lebovitz,[6] Chandrasekhar,[1] and Rosenkilde.[3]

Let us assume that the fluid drop, which is initially in a state of equilibrium, is slightly perturbed; and further that the ensuing motions are described by a Lagrangian displacement of the form

$$\xi(\underline{x})\, e^{\lambda t}\,, \tag{4.1}$$

where λ is a parameter whose characteristic values are to be determined. To the first order in ξ, the first variation of the moment equations (2.17) is

$$\begin{aligned} &\lambda^2 V_{i,j}^{*} - 2\lambda\Omega\epsilon_{i\ell 3} V_{\ell,j}^{*} \\ &\quad = \Omega^2\left[V_{i,j}^{*} + V_{j,i}\right] - \Omega^2\left[V_{j,3}^{*} + V_{3,j}^{*}\right]\delta_{i3} \\ &\qquad + \delta\Pi\,\delta_{ij} - 2\delta\mathcal{S}_{ij} + \delta\mathcal{W}_{ij}\,, \end{aligned} \tag{4.2}$$

where $\delta \mathcal{S}_{ij}$, $\delta \mathcal{W}_{ij}$, $\delta \Pi$ are variations of the associated quantities in Eq. (2.7). The quantities

$$V^*_{i,j} \equiv \int_V \rho \xi_i x_j \, d\tau \equiv \frac{1}{2} I^\circ V_{i,j} \quad , \tag{4.3}$$

where the symbol without the star is nondimensional, are known as the virials. The unsymmetrized virials, $V^*_{i,j}$ are related to the variation of the moment-of-inertia tensor, I_{ij}, by the equation

$$\delta \int_V \rho x_i x_j \, d\tau = V^*_{i,j} + V^*_{j,i} \equiv V^*_{ij} \tag{4.4}$$

Clearly, variations of higher-order moment equations would require the introduction of additional virials of higher order. However, the present considerations are limited to the nine moment equations of lowest order. The number of unknown parameters in the spatial dependence of the Lagrangian displacement cannot exceed the total number of moment equations being considered. Under these conditions, an appropriate choice for the form of ξ is the linear function

$$\xi \equiv L_{i,j} x_j \quad , \tag{4.5}$$

where the $L_{i,j}$ are undetermined nondimensional constants. This displacement is appropriate for an examination of the oscillations associated with the second-harmonic deformations of the equilibrium configurations of an incompressible fluid drop.

The specification of $\delta \Pi$ requires some supplementary assumption concerning the physical nature of the oscillations. For an incompressible

fluid, the Lagrangian displacement is required to be solenoidal in order to preserve the total volume. By supplementing the set of virial equations with the requirement that

$$0 = \nabla \cdot \underline{\xi} = L_{1,1} + L_{2,2} + L_{3,3} \quad , \tag{4.6}$$

it is possible to dispense with the evaluation of $\delta \Pi$ and eliminate it from the system of equations.

Expressions for the variations, $\delta \mathcal{W}_{ij}$ and $\delta \mathcal{A}_{ij}$, in terms of the nondimensional virials, $V_{i,j}$, are summarized in Appendix B. The necessary integrals have been evaluated over unperturbed spheroidal equilibrium configurations. As was the case in earlier investigations,[1,3,6] the virial equations (4.2) may be separated into three noncombining groups whose proper solutions are normal modes of the transverse-shear, the toroidal, and the pulsation types, respectively.

(A) Transverse-shear Mode

The equations that govern the transverse-shear mode depend upon the virials $V_{i,3}$ and $V_{3,i}$ (i=1,2). The associated displacement induces relative motion of the two hemispheres; the spheroid appears to oscillate about a diameter in the equatorial plane.

From the set (4.2), the four equations which describe the transverse-shear oscillations are

$$\begin{aligned}
\lambda^2 V_{1,3}^* - 2\lambda\Omega V_{2,3}^* &= -2\delta \mathcal{S}_{13} + \delta \mathcal{W}_{13} + \Omega^2 V_{1,3}^* \,, \\
\lambda^2 V_{3,1}^* &= -2\delta \mathcal{S}_{31} + \delta \mathcal{W}_{31} \,, \\
\lambda^2 V_{2,3}^* + 2\lambda\Omega V_{1,3}^* &= -2\delta \mathcal{S}_{23} + \delta \mathcal{W}_{23} + \Omega^2 V_{2,3}^* \,, \\
\lambda^2 V_{3,2}^* &= -2\delta \mathcal{S}_{32} + \delta \mathcal{W}_{32} \,.
\end{aligned} \tag{4.7}$$

By using Eqs. (B.11), (B.13), (B.14), and (B.18), one obtains

$$\begin{bmatrix}
\lambda^2 - \Omega^2 + M & M - \Omega^2 & -2\lambda\Omega & 0 \\
N & \lambda^2 + N & 0 & 0 \\
2\lambda\Omega & 0 & \lambda^2 - \Omega^2 + M & M - \Omega^2 \\
0 & 0 & N & \lambda^2 + N
\end{bmatrix}
\begin{bmatrix}
V_{1,3} \\ V_{3,1} \\ V_{2,3} \\ V_{3,2}
\end{bmatrix} = 0 \tag{4.8}$$

where

$$M \equiv \frac{15}{16}\omega_0^2\left[a_{13} - \frac{2\varkappa}{A_3}\left(2\frac{a_3^2 A_{13}^2}{A_1} + 3B_{133} - 2A_{13}\right)\right], \tag{4.9}$$

$$N \equiv \frac{15}{16}\omega_0^2\left[a_{13} - \frac{2\varkappa}{A_3}\left(2\frac{a_1^2 A_{13}^2}{A_1} + 3B_{133}\right)\right], \tag{4.10}$$

and the unit of frequency, ω_0 is defined by Eq. (A.10).

(B) Toroidal Mode

The equations that govern the toroidal mode depend upon the two virials $(V_{1,2}+V_{2,1})$ and $(V_{1,1}-V_{2,2})$. The associated displacement destroys the axial symmetry; the spheroid is transformed into a triaxial ellipsoid.

From the set (4.2), the two equations which describe the toroidal mode oscillation are

$$\lambda^2\left[V_{1,2}^{*}+V_{2,1}^{*}\right]+2\lambda\Omega\left[V_{1,1}^{*}-V_{2,2}\right]=-2\left[2\delta\mathcal{A}_{12}-\delta\mathcal{W}_{12}\right]+2\Omega^2V_{12}^{*},$$

$$\lambda^2\left[V_{1,1}^{*}-V_{2,2}\right]-2\lambda\Omega V_{12}^{*}=-2\left[\delta\mathcal{A}_{11}-\delta\mathcal{A}_{22}\right]+\left[\delta\mathcal{W}_{11}-\delta\mathcal{W}_{22}\right]+2\Omega^2\left[V_{1,1}^{*}-V_{2,2}^{*}\right]. \tag{4.11}$$

By using Eqs. (B.11), (B.12), (B.15), (B.17), and (B.19), one obtains

$$\begin{bmatrix}\lambda^2-2\left[\Omega^2-P\right] & 2\lambda\Omega\\ 2\lambda\Omega & \lambda^2-2\left[\Omega^2-P\right]\end{bmatrix}\begin{bmatrix}V_{1,2}+V_{2,1}\\ V_{1,1}-V_{2,2}\end{bmatrix}=0 \tag{4.12}$$

where

$$P\equiv\frac{15}{16}\omega_0^2\left[a_{11}-\frac{2\kappa}{A_3}B_{113}\right]. \tag{4.13}$$

(C) Pulsation Mode

The equations that govern the pulsation mode depend upon the virials $(V_{1,1}^* + V_{2,2}^*)$, $(V_{1,2}^* - V_{2,1}^*)$, and $V_{3,3}^*$. The associated displacement preserves the axial symmetry; the spheroid is transformed into another spheroid having a slightly different elongation.

From the set (4.2), the equations which describe the pulsation oscillation are

$$\lambda^2\left[V_{1,2}^* - V_{2,1}^*\right] - 2\lambda\Omega\left[V_{1,1}^* + V_{2,2}^*\right] = 0 ,$$

$$\lambda^2\left[V_{1,1}^* + V_{2,2}^* - 2V_{3,3}^*\right] + 2\lambda\Omega\left[V_{1,2}^* - V_{2,1}^*\right] - 2\Omega^2\left[V_{1,1}^* + V_{2,2}^*\right] \qquad (4.14)$$

$$= -2\left[\delta\mathcal{A}_{11} + \delta\mathcal{A}_{22} - 2\delta\mathcal{A}_{33}\right] + \left[\delta W_{11} + \delta W_{22} - 2\delta W_{33}\right] .$$

The second of these results from the elimination of $\delta\Pi$ from the set by using the third diagonal equation $(i = j = 3)$. This process does not eliminate $V_{3,3}^*$ so it is necessary to supplement Eqs. (4.14) with the algebraic relation

$$V_{3,3}^* = -a_3^2 a_1^{-2}\left[V_{1,1}^* + V_{2,2}^*\right] , \qquad (4.15)$$

which is equivalent to the divergence condition (4.6). By using Eqs. (B.16) and (B.20), one obtains

$$\begin{bmatrix} \lambda^2\left[1+2a_3^2a_1^{-2}\right]+2Q-2\Omega^2 & 2\lambda\Omega \\ -2\lambda\Omega & \lambda^2 \end{bmatrix} \begin{bmatrix} V_{1,1}+V_{2,2} \\ V_{1,2}-V_{2,1} \end{bmatrix} = 0, \quad (4.16)$$

where

$$Q \equiv \frac{15}{16}\omega_o^2\left[Q_s - 6\chi a_1^2 A_3^{-1} Q_c\right] \quad (4.17)$$

with

$$Q_s \equiv 2a_{11} - a_{13} + a_3^2 a_1^{-2}\left[3a_{33} - a_{13}\right] \quad (4.18)$$

and

$$Q_c \equiv 6B_{13}^2 A_3^{-1} + 2a_1^2 B_{113} - 3a_3^2 B_{133} \; . \quad (4.19)$$

Altogether there are a total of nine, homogeneous, linear equations as required for the determination of the nine unknown virials, $V_{i,j}$. Eight of these (excepting Eq. (4.15) are quadratic in λ^2 indicating that there are a total of sixteen characteristic frequencies.

V. CHARACTERISTIC FREQUENCIES AND INSTABILITY

The normal modes of oscillation of a liquid drop correspond to the proper solutions of three non-combining groups (4.8), (4.12) and (4.15) of equations derived from the virial equation (4.2) by subjecting a spheroidal equilibrium configuration to a Lagrangian displacement (4.1) having an exponential time dependence, $\exp(\lambda t)$. Each group of equations yields a characteristic polynomial in λ^2 whose coefficients are real functions of the equilibrium elongation. It is convenient to replace λ^2 by $-\omega^2$, so that real characteristic roots, ω, of these polynomials correspond to undamped oscillatory, stable motion, while pairs of conjugate complex roots reveal the possibility of exponentially growing deformations associated with unstable motion. Thus, by examining the nature of these characteristic roots as a function of the elongation, it is possible to identify those equilibrium configurations that are unstable.

(A) Torrodial Mode

The system of equations (4.12) yields a characteristic polynomial of fourth degree in ω that may be separated into two physically equivalent quadratic factors

$$\omega^2 \pm 2\Omega\omega + 2\left[\Omega^2 - P\right] , \tag{5.1}$$

which differ only in the sign (and hence the direction) of the angular speed of rotation, Ω .

These characteristic polynomials have a pair of conjugate complex roots if

$$\Omega^2 > 2P . \tag{5.2}$$

By using the definitions (4.13), (A.10), and (A.12), this inequality becomes

$$y > a_1^4\left(a_{11} - 2A_3^{-1} B_{113} x\right) . \tag{5.3}$$

Configurations possessing sufficient angular momentum, y , to simultaneously satisfy both the equilibrium relation (3.13) and the inequality (5.3) lie in the region above the curve LMN in Fig. 2. These configurations are unstable. Infinitesimal deformations will grow exponentially via overstable oscillations (in the sense of Eddington).[11]

Further examination of the toroidal mode reveals another important property. Each polynomial (5.1) has a nontrivial zero characteristic root in the particular case that

$$\Omega^2 = P \,, \tag{5.4}$$

which is equivalent to the requirement that

$$y = \frac{1}{2} a_1^4 \left[a_{11} - 2 A_3^{-1} B_{113} \varkappa \right] . \tag{5.5}$$

Those spheroidal configurations which possess sufficient angular momentum, y , to simultaneously satisfy both the equilibrium relation (3.13) and the requirement (5.5) lie along the curve BCF in Fig. 2.

This curve BCF in Fig. 2 is a curve of bifurcation (in the terminology of Poincare).[12] The differential equations corresponding to the system (4.12) possess a time independent solution when the condition (5.4) is satisfied. The resulting displacement transforms an axisymmetric spheroidal configuration into a genuine triaxial ellipsoidal equilibrium configuration. These triaxial shapes first become possible figures of equilibrium when the angular momentum equals or exceeds the values of along this curve of bifurcation.

The existence of these triaxial equilibrium configurations can be examined from another viewpoint. Reconsider the pair of equilibrium relations (3.12). By using the definitions (A.11) and (A.12) for the parameters $\varkappa$ and y , the sum of these two relations becomes

FIG. 2. Critical curves separating regions of unstable configurations from possibly stable ones are shown superimposed upon the background of equilibrium relations displayed in FIG. 1. Stable configurations are restricted to the closed region ABCDEA.

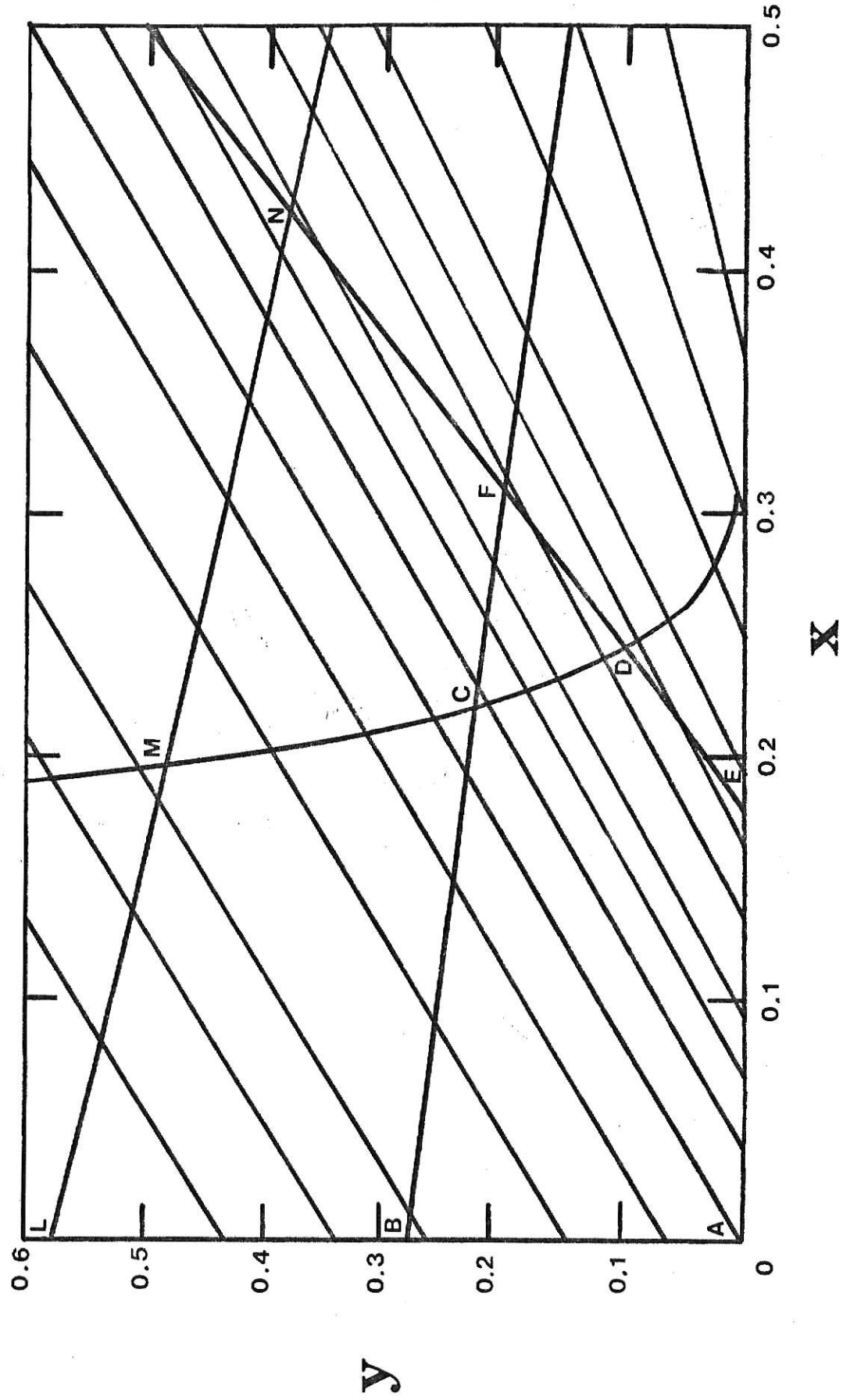
0.6
0.5
0.4
0.3
0.2
0.1
0
0.1
0.2
0.3
0.4
0.5
y
x
L
M
N
B
C
F
D
E
A

$$4y\left[a_1^2+a_2^2\right]^{-1} = \frac{1}{2}\left[2a_3 - a_1 - a_2\right] - A_3^{-1}\left[a_1^2 A_{13} + a_2^2 A_{23} - 6a_3^2 A_{33}\right]\varkappa , \tag{5.6}$$

and the difference becomes

$$4y\left[a_1^2+a_2^2\right]^{-2} = \frac{1}{2} a_{12} - A_3^{-1} B_{123}\varkappa , \tag{5.7}$$

after the cancellation of a common factor of $(a_1^2 - a_2^2)$. This pair of equations is equivalent to the pair (3.12). In the limit that a_1 approaches a_2 the first of these relations reduces to the spheroidal equilibrium relation (3.13), while the second reduces to condition (5.5) which implies the existence of the zero characteristic root. This limiting procedure confirms the existence of new sequences of triaxial equilibrium configurations which bifurcate from the axisymmetric configurations provided that the angular momentum exceeds certain critical values.

The situation here is reminiscent of the bifurcation of the classical, self-gravitating Jacobi ellipsoids from the equilibrium sequence of Maclaurin spheroids.[5] Similar behavior also is exhibited by a rotating liquid drop[1] ($\varkappa = 0$) and a rotating, homogeneously charged atomic nucleus.[13]

In the absence of <u>any</u> dissipative mechanism, the spheroidal configurations which lie in the region between the curve of bifurcation BCF and the curve of overstability LMN are expected to be stable with respect to second-harmonic displacements associated with the toroidal mode. However, the inclusion of any viscous stress or radiation reaction, no

matter how small, is expected to induce secular instability in accordance with the behavior of the slightly viscous Maclaurin spheroids investigated by Rosenkilde[14] and the rotating, charged liquid drops investigated by Stettner.[15] Thus any realistic axisymmetric configurations are expected to be (secularly) unstable above the curve of bifurcation.

(B) Pulsation Mode

The system of equations (4.16) yields a characteristic polynomial of fourth degree which has two trivially zero roots that correspond to trivial rigid body rotations in opposite directions about the a_3 axis. The remaining quadratic factor is

$$\omega^2\left[1+2\,a_3^2\,a_1^{-2}\right]-2\Omega^2-2Q. \tag{5.8}$$

This factor yields purely imaginary roots if

$$\Omega^2+Q<0, \tag{5.8}$$

which is equivalent to the condition

$$3\,a_1^2A_3^{-1}Q_c\,\varkappa>\frac{1}{2}\,a_1^4\,Q_s+\gamma, \tag{5.9}$$

where Q_s and Q_c are defined by Eqs. (4.17) and (4.18), respectively. Those configurations which possess sufficient electrostatic energy to simultaneously satisfy both the equilibrium relation (3.13) and the inequality (5.9) lie in the region to the right of the curve EDFN in Fig. 2. These configurations are unstable. Infinitesimal deformations will grow exponentially with time.

It is worth noting that the equilibrium conditions are such that the required strength of the applied electric field, which is characterized by the parameter $FR^{1/2}T^{-1/2}$ defined by equation (A.14), attains a

relative maximum for a given angular momentum, γ , along the curve EDFN. Consequently, for values of the electric field which are less than this maximum value, there exist two prolate spheroidal equilibrium configurations of which the more elongated one is unstable. This conclusion agrees with the results of earlier investigations of the limiting case with no rotation.[2,3] Efforts to avoid confusion over this dichotomy led to the definition of the electrical parameter χ being used in the present considerations. Corresponding parameters used in other investigations are compared in Appendix A.

(C) Transverse-Shear Mode

The system of equations (4.7) yields a characteristic polynomial of eighth degree which has two trivially zero roots that correspond to trivial rigid body rotations about the a_1 and a_2 axes. The remaining sixth degree polynomial in ω may be separated into two physically equivalent cubic factors

$$\omega^3 \pm 2\Omega\omega^2 + \left[\Omega^2 - M - N\right]\omega \pm 2\Omega N = 0, \qquad (5.10)$$

which differ only in the sign of the angular speed of rotation, Ω .

These characteristic polynomials have a pair of conjugate complex roots if the condition

$$\Omega^2\left[\Omega^2 - 9(M-2N)\right]^2 > \left[\Omega^2 + 3(M+N)\right]^3, \qquad (5.11)$$

is satisfied. Configurations which possess sufficient electrostatic energy, $\mathcal{K}$, to simultaneously satisfy both the equilibrium relation (3.13) and the inequality (5.11) lie in the region to the right of the curve DCM in Fig. 2. These configurations are unstable.

(D) Combined Mode Analysis

The foregoing analysis of the normal modes of oscillation associated with second-harmonic deformations restricts stable spheroidal equilibrium configurations to the closed polygon ABCDEA in the $\alpha-\gamma$ configuration plane shown in Fig. 2. Configurations which lie outside this region are definitely unstable, while those within this region may be stable pending an examination of other, perhaps higher harmonic, deformations.

VI. NUMERICAL RESULTS AND COMPARISONS

The numerical calculations required to construct the curves displayed Figs. 1 and 2 were performed on a programable Hewlett-Packard desk calculator, model HP 9100B, with an extended memory unit, model 9101A. The results of these calculations are presented in Tables I-VI.

Table I contains the slopes and intercepts of the equilibrium lines as a function of the elongation, k . Selected lines are displayed in Fig. 1. The y -intercepts for oblate shapes ($k < 1$) agree with those obtained by Rosenkilde:[13] the x -intercepts for prolate shapes ($k > 1$) agree with those obtained by Rosenkilde.[3]

Tables II-V contain data for the "critical" curves associated with the normal modes of oscillation described in Section V. These curves are displayed in Fig. 2.

Table VI contains the values of x , y , and k associated with the points of intersection of the critical curves with each other and with the coordinate axes. The parameters at E agree with those obtained by Rosenkilde:[3] the parameters at B and L agree with those obtained by Rosenkilde.[13]

It is of interest to examine the domain of applicability of the ellipsoidal approximation by comparing the present results with the earlier ones obtained for certain limiting cases by using more exact equilibrium shapes. On the oblate side ($k < 1$), the exact figures of equilibrium in the limit of the zero electric field ($x \to 0$) have been obtained analytically by Rayleigh[10] and Chandrasekhar.[1] The points of

intersection, B and L, were obtained for the exact shapes by Chandrasekhar. He showed that the point B corresponds to $(y, k) = (0.28338, 0.67139)$ and the point L corresponds to $(y, k) = (0.5930, 0.4924)$. These values are to be compared with the corresponding ones in Table VI. The exact shapes are flatter in the polar regions than the corresponding ellipsoidal shapes and have a dimple there for values of $y > 0.74306$ and $k < 0.43118$. Consequently, the ellipsoidal approximation cannot be valid beyond these values.

The situation on the prolate side ($k > 1$) is less certain. Contrary to earlier expectations, exact analytical expressions for the figures of equilibrium in the limit of zero angular momentum ($y \to 0$) are unknown. These can only be obtained through an exact treatment of both the interfacial tension and the electrical stress. The choice, here, of a spheroidal shape as a first approximation permits an exact treatment of the electrical stress but ultimately introduces an error by way of the surface tension. Alternatively, Garton and Krasucki[16] give an exact treatment of the interfacial tension but introduce an error in the treatment of the electrical stress by assuming an uniform field within their dielectric. The resulting external field, and hence the required exterior electrical stress, obtained by using the Maxwell boundary conditions, will still be in error even in the conducting limit (in which the dielectric permeability approaches infinity). However, Garton and Krasucki show that their equilibrium shapes differ little from the corresponding spheroids at least for small electric fields ($\chi \ll 0.18$). At the other extreme near the unstable point E in Fig. 2 ($\chi \approx 0.18$), Taylor[2] has argued that the elongated ends of a drop develop conical

points prior to the appearance of a narrow jet. Such behavoir clearly involves harmonics of order greater than two.

It is possible to calculate the exact shape of a charged drop in an electric field by using the iterative numerical procedure described by Brazier-Smith.[17] For the particular case of zero charge of interest here, he showed that the exact shapes were slightly more elongated than the corresponding spheroids, but that the spheroidal approximation was quite good unless the parameters were within a few per cent of those associated with the unstable point at E in Fig. 2. Indeed, by associating this point with the point at which his iterative procedure ceased to converge, he predicted that the critical elongation should be 1.83 at which the electrical parameter, $F(R/T)^{1/2}$, should be 1.603. (See Appendix A, Eq. A.15, for the relation between this electrical parameter and the χ being used in the present analysis). The spheroidal approximation used together with the present moment method yields $F(R/T)^{1/2} = 1.6028$. Of course this is only slightly more accurate than the value of 1.625 originally obtained by Taylor[1] who very simply, and effectively, balanced the stresses just at the poles and at the equator of the spheroid.

The situation for rotating drops is much the same. The equilibrium shapes obtained by Habip, Siekmann, and Chang[4] were derived by accepting the analysis of the electrical stress as given by Garton and Krasucki,[16] and hence, are subject to the same criticism. The electrical field within their dielectric drop certainly cannot be uniform after the appearance of the polar dimples at high angular momentum ($y > 0.75$). Fortunately, the present analysis predicts that instability will set in long before such a configuration can be attained.

Among the possibly stable configurations within the polygon ABCDEA in Fig. 2, the points B (k = 0.6858) and E (k = 1.8391) correspond to the extreme values of the elongation. Within these limits, there appears to be considerable justification for the ellipsoidal approximation. The qualitative features of Fig. 2 are not expected to change radically with the inclusion of additional higher moments or harmonics in the approximate equilibrium shape.

VII. CONCLUDING REMARKS

The present analysis may be extended in several directions. Isolated rotating configurations having finite dielectric permeability can be investigated within the context of the ellipsoidal approximation by using the moment method applied here. The properties of the triaxial configurations, predicted here, are also accessible with these techniques. The inclusion of an external dielectric medium will add complexity. An analysis of the radiation reaction, expected to have dipole character here, should be possible following the methods outlined by Stettner.[15] The more difficult tasks of obtaining exact axisymmetric figures of equilibrium for zero angular momentum and exact triaxial figures in zero electric field remain for the future.

APPENDIX A: THE DIMENSIONAL UNITS AND THE PARAMETERS $\varkappa$ AND γ

It is necessary to establish definite units of length, frequency, angular momentum and energy associated with the ellipsoidal figure

$$\sum_{i=1}^{3} \varkappa_i^2 \left[a_i^*\right]^{-2} = 1 \,, \tag{A.1}$$

having semiaxes a_1^*, a_2^*, and a_3^*.

Introduce a reference sphere which has the same density ρ and volume V as the ellipsoidal configuration. The radius,

$$R \equiv \left[a_1^* a_2^* a_3^*\right]^{1/3} \,, \tag{A.2}$$

of this sphere is a convenient unit of length. The non dimensional semi-axes of the ellipsoid may be denoted by

$$a_i \equiv a_i^* R^{-1} \qquad (i = 1, 2, 3) \tag{A.3}$$

The moment of inertia of this reference sphere is

$$I^\circ \equiv \frac{8\pi}{15} \rho R^5 \,. \tag{A.4}$$

The angular momentum, H, of a homogeneous ellipsoid which rotates uniformly with the angular speed Ω about the axis a_3 is

$$H = \frac{1}{2} I^{\circ}\left[a_1^2 + a_2^2\right]\Omega \,. \tag{A.5}$$

The electrostatic energy,* W, associated with an uniform dielectric ellipsoid having the electrical permeability ϵ and the volume V and which is situated in an uniform applied electric field F is given by the general expression

$$W = -\frac{1}{2}\int_V \underline{E}\cdot\underline{P}\, d\tau \,, \tag{A.6}$$

where the uniform polarization $\underline{P}$ has the components[3]

$$4\pi P_i = \left[\epsilon - 1\right] F_i \left[1 + \frac{1}{2}(\epsilon - 1) A_i\right]^{-1} \quad (i = 1,2,3) \,, \tag{A.7}$$

(The indexed-symbols, A_i, are defined in Appendix B.) For the particular case of a conducting ellipsoid (obtained in the limit $\epsilon \longrightarrow \infty$) whose semiaxis, a_3, is parallel to the applied electric field, it is useful to define the quantity

$$E_c \equiv F^2 R^3 \left[3A_3\right]^{-1} = |W| \,. \tag{A.8}$$

The surface energy, E_s°, of the liquid reference sphere having a constant surface tension T is

$$E_s^{\circ} = 4\pi R^2 T \,. \tag{A.9}$$

*Gaussian units are assumed for all electrical quantities.

A convenient unit of frequency is

$$\omega_o = \left[8T\right]^{1/2}\left[\rho R^3\right]^{-1/2} = \left[16 E_s^o\right]^{1/2}\left[15 I^o\right]^{-1/2}, \qquad (A.10)$$

which is associated with the second-harmonic deformations of the uniform liquid reference sphere.

It is further useful to introduce two additional non-dimensional parameters. The electrical parameter,

$$\chi \equiv E_c\left[E_s^o\right]^{-1} = F^2 R\left[12\pi T A_3\right]^{-1}, \qquad (A.11)$$

is the electrostatic energy expressed in units of the surface energy of the reference sphere. The rotational parameter,

$$y \equiv H^2\left[2 I^o E_s^o\right]^{-1} = I^o\left[a_1^2 + a_2^2\right]\Omega^2\left[8 E_s^o\right]^{-1}, \qquad (A.12)$$

is the square of the angualr momentum expressed in units associated with the reference sphere.

The rotational parameter y defined here has long been utilized in investigations of spheroidal nuclei[13] rotating about the axis of symmetry, a_3. It was adopted because it increases monotonically with the elongation, a_3/a_1, along a sequence of equilibrium congigurations characterized by a given mass and charge, whereas the more natural mathematical parameter,

$$\rho\Omega^2 R^3\left[2T\right]^{-1} = 15\, y\left[2\, a_1^4\right]^{-1}, \qquad (A.13)$$

utilized by Habip, et. al.,[4] attains a maximum value along such a sequence. The situation here is reminiscent of the contrasting characterizations of the sequence of self-gravitating Maclaurin spheroids in terms of either increasing angular momentum or changing angular speed of rotation.[5]

The electrical parameter $\varkappa$ defined here differs from the non-dimensional parameters commonly utilized in earlier investigations. It was adopted in the present case because it increases monotonically with the elongation along a sequence of equilibrium configurations characterized by a given angular momentum and mass. In this respect it is similar to the parameter

$$\left[L k_1\right] \equiv 6\varkappa\left[A_3\right]^{-1}, \tag{A.14}$$

defined by Habip, et. al.[4] The more natural mathematical parameter

$$F R^{1/2} T^{-1/2} = \left[12\pi A_3 \varkappa\right]^{1/2}, \tag{A.15}$$

which was used by Taylor[2] and Rosenkilde,[3] has the disadvantage of not being monotonic in the present case. For a fixed angular momentum, the applied electric field, F, attains a maximum value when the equilibrium configurations become unstable with respect to the pulsation mode (cf. Section VB). However this disadvantage is offset by the utility in comparing theory with experiment because of the absence of the shape-dependent factor, A_3, in the definition.

APPENDIX B: TENSORIAL QUANTITIES FOR ELLIPSOIDS

Expressions are needed for the various tensorial quantities which appear in the moment equation (2.7) and its variation (4.2) in the particular case that the equilibrium configurations are assumed to be homogeneous ellipsoids with nondimensional semiaxes a_1, a_2, and a_3. (All dimensional units are defined in Appendix A.) The summation convention over repeated indices does not apply in Appendix B.

The diagonal components of the moment of inertia tensor are

$$I_{ii} = \frac{1}{2} I^{\circ} a_i^2 \qquad (i = 1, 2, 3), \tag{B.1}$$

where the moment, I°, is defined in Appendix A.

The electrostatic contributions contained in the tensor, $\mathcal{W}_{ij}$, defined by equation (2.18), have been evaluated by Rosenkilde[3] for ellipsoidal surfaces enclosing an incompressible dielectric fluid drop situated in an uniform electric field. The components involve a certain class of elliptic integrals which is well known in the potential theory of ellipsoids. These integrals will be denoted by the multi-indexed symbols A_i, A_{ij}, B_{ij}, etc., where in general

$$A_{ijk\cdots} \equiv \int_0^{\infty} f(u)\, du \tag{B.2}$$

and

$$B_{ijk\cdots} \equiv \int_0^\infty u\, f(u)\, du \tag{B.3}$$

with

$$\left[f(z)\right]^{-1} \equiv \left[(a_1^2+z)(a_2^2+z)(a_3^2+z)\right]^{1/2} (a_i^2+z)(a_j^2+z)(a_k^2+z)\cdots , \tag{B.4}$$

for arbitrary combinations of (i, j, k). Chandrasekhar[5] has given a more complete summary of the properties of these integrals including the algebraic recursion relations utilized in making reductions and numerical computations.

In the present context, the components of $\mathcal{W}_{ij}$ are required for a conducting fluid drop in an uniform electric field. The necessary expressions may be obtained from the corresponding ones for the dielectric case by taking the limit as the dielectric permeability ϵ approaches infinity (cf. Landau & Lifsitz).[7] The general expressions obtained by Rosenkilde[3] may be further simplified by making use of the necessary orientation of the electric field (cf. Section III). The resulting combinations required here are

$$\mathcal{W}_{11} - \mathcal{W}_{22} = E_c A_3^{-1}\left[a_1^2 A_{13} - 3 a_3^2 A_{33}\right] \tag{B.5}$$

and

$$\mathcal{W}_{22} - \mathcal{W}_{33} = E_c A_3^{-1}\left[a_2^2 A_{23} - 3 a_3^2 A_{33}\right], \tag{B.6}$$

where the electrostatic energy, E_c, is defined in Appendix A.

The surface-energy tensor, $\mathcal{A}_{ij}$, which is defined by equation (2.13), has been evaluated for an ellipsoidal surface by Rosenkilde.[9] The components involve another class of elliptic integrals denoted by the multi-indexed symbols a_i, a_{ij}, and $\mathcal{B}_{ij}$, etc., where in general

$$a_{ijk\cdots} \equiv \int_0^\infty f(t^2)\, dt \tag{B.7}$$

and

$$\mathcal{B}_{ijk} \equiv \int_0^\infty t^2 f(t^2)\, dt \tag{B.8}$$

with $f(z)$ defined by equation (B.4). This class of integrals also satisfies algebraic recursion relations.[9]

The particular combinations of the components of $\mathcal{A}_{ij}$ required here are

$$2\mathcal{A}_{11} - 2\mathcal{A}_{33} = \frac{1}{2} E_s^\circ [a_3 - a_1] \tag{B.9}$$

and

$$2\mathcal{A}_{22} - 2\mathcal{A}_{33} = \frac{1}{2} E_s^\circ [a_3 - a_2], \tag{B.10}$$

where the surface energy, E_s°, is defined in Appendix A.

All of the above expressions are also valid if two semimajor axes of the ellipsoid are identical. For a spheroid with $a_1 = a_2 \neq a_3$,

the appropriate expressions for $\mathcal{W}_{ij}$ and $\mathcal{J}_{ij}$ may be obtained by replacing a_2 by a_1 wherever it appears. For example, A_{23} and a_2 would become A_{13} and a_1, respectively. Then the right hand sides of each pair of equations (B.5), (B.6) and (B.9), (B.10) become identical.

The specification of the variations in the virial equations (4.2) in terms of the nondimensional virials,

$$V_{i,j} = L_{i,j}\, a_j^2 , \qquad \text{(no sum)} \qquad \text{(B.11)}$$

defined by equation (4.2) has been given in the general ellipsoidal case by Rosenkilde[3,9] in different units than are being employed here. Since the present investigation is limited to conducting, spheroidal equilibrium configurations, it is useful to list the particular combinations in that limit that are needed here.

The electrostatic contributions contained in the variation that are required here for an incompressible, conducting, spheroidal drop may be obtained from the corresponding general expressions in the case of a dielectric drop[3] by taking the limit as the dielectric permeability ϵ approaches infinity. Further simplification is obtained by setting $a_2 = a_1$, by making use of the orientation of the unperturbed applied electric field ($F_1 = F_2 = 0 \neq F_3$), and by using the divergence condition (4.15). The resulting combinations required here are:

$$\delta\mathcal{W}_{12} = \delta\mathcal{W}_{21} = E_c A_3^{-1} B_{113} V_{12} \qquad \text{(B.12)}$$

$$\delta^2 w_{i3} = E_c A_3^{-1}\left[2 a_3^2 A_1^{-1} A_{13}^2 + 3 B_{133} - 2 A_{13}\right] V_{i3} \qquad (B.13)$$

$$\delta^2 w_{3j} = E_c A_3^{-1}\left[2 a_1^2 A_1^{-1} A_{13}^2 + 3 B_{133}\right] V_{3j} \quad \begin{matrix}(i=1,2)\\ (j=1,2)\end{matrix}, \qquad (B.14)$$

$$\delta^2 w_{11} - \delta^2 w_{22} = 2 E_c A_3^{-1} B_{113}\left[V_{1,1} - V_{2,2}\right], \qquad (B.15)$$

$$\begin{aligned}\delta^2 w_{11} + \delta^2 w_{22} - 2\delta^2 w_{33} = \\ 2E_c A_3^{-1}\Big[\left[2 a_1^2 B_{113} - 3 a_3^2 B_{133}\right]\left[\left(V_{1,1}+V_{2,2}\right) a_1^2 - 2 V_{3,3}\, a_3^{-2}\right] \\ + 2 A_3^{-1}\left[a_1^2 A_{13} - 3 a_3^2 A_{33}\right]\left[A_{13}\left(V_{1,1}+V_{2,2}\right) + 3 A_{33} V_{3,3}\right]\Big].\end{aligned} \qquad (B.16)$$

Rosenkilde[9] also developed the needed variations of the surface-energy tensor, $\delta \mathcal{A}_{ij}$. The required combinations are:

$$2\delta \mathcal{A}_{12} = 2\delta \mathcal{A}_{21} = \frac{1}{2} E_s^{\circ} a_{11} V_{12}, \qquad (B.17)$$

$$2\delta \mathcal{A}_{i3} = 2\delta \mathcal{A}_{3i} = \frac{1}{2} E_s^{\circ} a_{13} V_{i3} \quad (i=1,2), \qquad (B.18)$$

$$2\left[\delta \mathcal{A}_{11} - \delta \mathcal{A}_{22}\right] = \frac{1}{2} E_s^{\circ} a_{11}\left[V_{1,1} - V_{2,2}\right], \qquad (B.19)$$

$$\begin{aligned}2\left[\delta \mathcal{A}_{11} + \delta \mathcal{A}_{22} - 2\delta \mathcal{A}_{33}\right] = \\ \frac{1}{2} E_s^{\circ}\Big[\left[2 a_{11} - a_1^{-2} a_3^2 a_{13}\right]\left[V_{1,1} + V_{2,2}\right] \\ - \left[3 a_{33} - a_3^{-2} a_1^2 a_{13}\right] V_{3,3}\Big].\end{aligned} \qquad (B.20)$$

TABLE I. Equilibrium lines.

k	y-intercept	Slope	k	x-intercept	Slope
0.50	0.6924	1.2598	1.1	0.0395	1.1814
0.55	0.5478	1.2596	1.2	0.0709	1.1625
0.60	0.4326	1.2573	1.3	0.0966	1.1435
0.65	0.3393	1.2532	1.4	0.1178	1.1246
0.70	0.2627	1.2478	1.5	0.1356	1.1061
0.75	0.1991	1.2413	1.6	0.1508	1.0879
0.80	0.1456	1.2341	1.7	0.1640	1.0702
0.90	0.0618	1.2178	1.8	0.1755	1.0530
1.00	0.0000	1.2000	1.9	0.1856	1.0363
			2.0	0.1945	1.0200
			3.0	0.2500	0.8835
			5.0	0.2993	0.7072
			10.0	0.3600	0.4952

TABLE II. Bifurcation curve BCF.

α	y	k
0.00	0.2830	0.6858
0.05	0.2702	0.7424
0.10	0.2574	0.8119
0.15	0.2447	0.8998
0.20	0.2319	1.0144
0.25	0.2191	1.1708
0.30	0.2060	1.3957
0.35	0.1926	1.7404
0.40	0.1786	2.3040
0.45	0.1637	3.2482
0.50	0.1488	4.7423

TABLE III. Overstability curve LMN.

α	y	k
0.00	0.5795	0.5380
0.05	0.5550	0.5729
0.10	0.5306	0.6138
0.15	0.5063	0.6626
0.20	0.4824	0.7219
0.25	0.4588	0.7955
0.30	0.4356	0.8892
0.35	0.4129	1.0121
0.40	0.3908	1.1792
0.45	0.3694	1.4151
0.50	0.3488	1.7591

TABIE IV. Pulsation

curve EDFN.

x	y	k
0.1796	0.00	1.8390
0.2134	0.05	1.7211
0.2464	0.10	1.6237
0.2787	0.15	1.5412
0.3105	0.20	1.4700
0.3418	0.25	1.4078
0.3728	0.30	1.3526
0.4036	0.35	1.3032
0.4340	0.40	1.2587
0.4643	0.45	1.2183
0.4944	0.50	1.1813

TABLE V. Transverse-Shear curve DCM.

x	y	k
0.1896	0.6000	0.6368
0.1925	0.5500	0.6685
0.1955	0.5000	0.7048
0.1989	0.4500	0.7467
0.2027	0.4000	0.7958
0.2069	0.3500	0.8547
0.2116	0.3000	0.9270
0.2171	0.2500	1.0189
0.2237	0.2000	1.1413
0.2319	0.1500	1.3167
0.2430	0.1000	1.6017
0.2500	0.0770	1.8124
0.3000	0.0113	4.2622
0.3500	0.0029	8.4477

TABLE VI. Intersections of critical curves.

Point	λ	y	k
B	0.0000	0.2830	0.6858
L	0.0000	0.5795	0.5380
E	0.1796	0.0000	1.8390
D	0.2440	0.0963	1.6302
C	0.2200	0.2268	1.0710
M	0.1966	0.4840	0.7175
F	0.3123	0.2028	1.4664
N	0.4225	0.3811	1.2750

REFERENCES

[1]S. Chandrasekhar, Proc. Roy. Soc. A286, 1, (1965).

[2]G. I. Taylor, Proc. Roy. Soc. A280, 383, (1964).

[3]C. E. Rosenkilde, Proc. Roy. Soc. A312, 473, (1969).

[4]Habip, Siekmann, & Chang Acta Mechanica IV, 107, (1966).

[5]S. Chandrasekhar, "Ellipsoidal Figures of Equilibirum." New Haven: Yale University Press, (1969).

[6]N. R. Lebovitz, Astrophys. J. 134, 500, (1961).

[7]Landau, & Lifshitz, "Electrodynamics of Continuous Media." Oxford: Pergamon Press, (1960).

[8]S. Chandrasekhar, "Hydrodynamic and Hydromagnetic Stability." Oxford: Clarendon Press, (1961).

[9]C. E. Rosenkilde, J. Math. Phys. 8, 88, (1967).

[10]Lord Rayleigh, Phil. Mag. 28, 161, (1914).

[11]A. S. Eddington, Internal Constitution of the Stars. New York: Dover Publications, Inc., (1959), p. 201.

[12]H. Pomcare, Acta Math. 7, 259, (1885).

[13]C. E. Rosenkilde, J. Math. Phys. 8, 98, (1967).

[14]C. E. Rosenkilde, Astrophys. J. 148, 825, (1967).

[15]R. Stettner, J. Math. Phys. 12, 1159, (1971).

[16]C. G. Garton & Z. Krasucki, Proc. Roy Soc. A280, 211 (1964).

[17]P. R. Brazier-Smith, Phys. Fluids. 14, 1, (1971).

ON THE SHAPE AND STABILITY OF A CONDUCTING FLUID DROP ROTATING IN AN ELECTRIC FIELD

by

RUSSEL R. RANDALL

B.A., Kansas State Teachers College, 1970

AN ABSTRACT OF A MASTER'S THESIS

submitted in partial fulfillment of the

requirements for the degree

MASTER OF SCIENCE

Department of Physics

KANSAS STATE UNIVERSITY
Manhattan, Kansas

1973

ABSTRACT

The equilibrium and stability of an isolated, inviscid, incompressible, neutral conducting fluid drop whose axis of uniform rotation coincides with an uniform applied electric field are examined by using an appropriate extension of the virial method developed by Chadrasekhar. Rotating spherical, spheroidal, and ellipsoidal equilibrium shapes are shown to satisfy the first twelve moment equations. A linear, one-parameter (the elongation) family of equilibrium curves relates the electrostatic energy, $\mathcal{X}$, to the square of angular momentum, $\mathcal{Y}$, of a given spheroidal shape. Conditions for the onset of instability, obtained from a linearized normal-mode analysis associated with second-harmonic deformations, restrict stable spheroidal configurations to a closed region of this $\mathcal{X}-\mathcal{Y}$ configuration plane. Comparisons are made with the classical, self-gravitating Maclaurian spheroids and Jacobi ellipsoids.